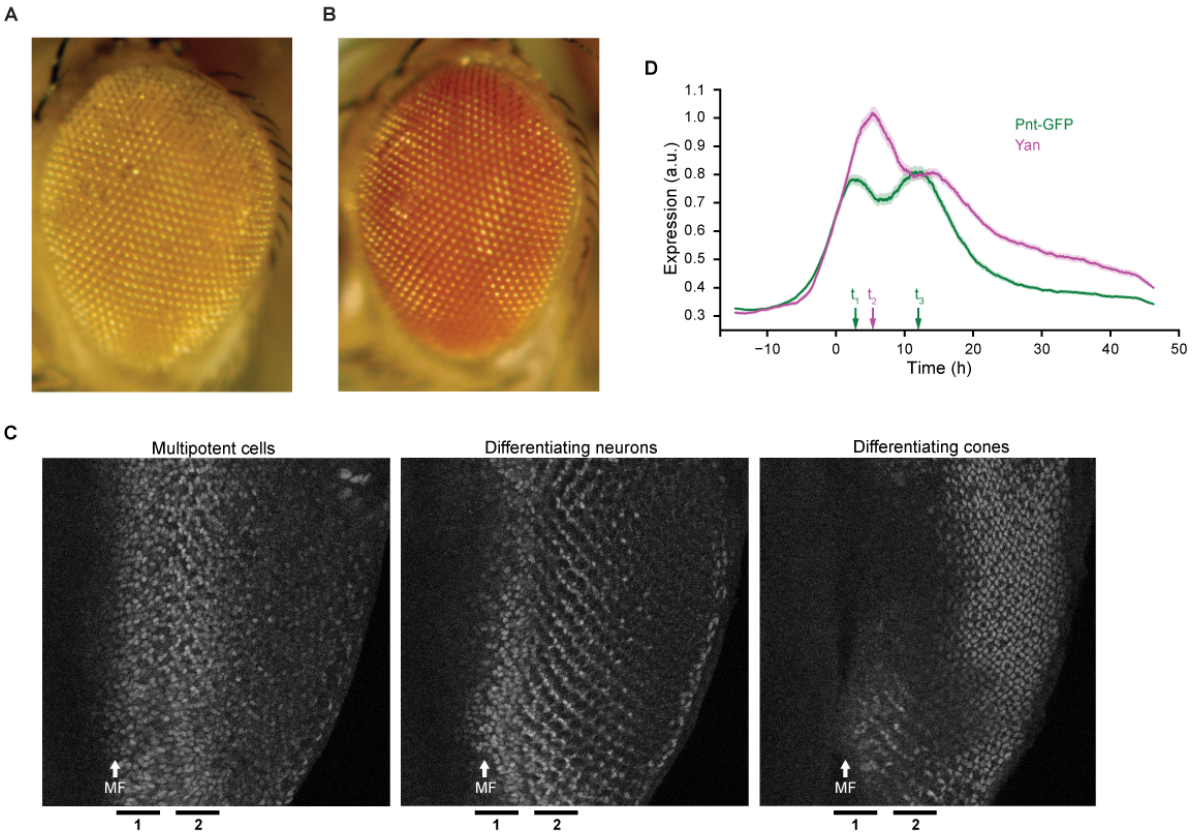

Figure S1:

(A,B) Adult eyes of flies carrying (A) one or (B) two copies of the recombineered Pnt-GFP transgene under a *pnt* null mutant background. Note the wildtype retina patterning under both rescue conditions.

(C) Maximum intensity projections of Pnt-GFP fluorescence across layers spanning multipotent cells, differentiating R cells, and differentiating cones. White arrow denotes morphogenetic furrow. Black bars denote first and second periods of elevated Pnt-GFP expression.

(D) Simultaneous Pnt-GFP (green) and Yan (magenta) expression dynamics in multipotent cells. Lines are smoothed moving averages across 500 sequential progenitors, shaded regions are bootstrapped 95% confidence intervals for the mean. Arrows indicate the times at which local maxima occur.

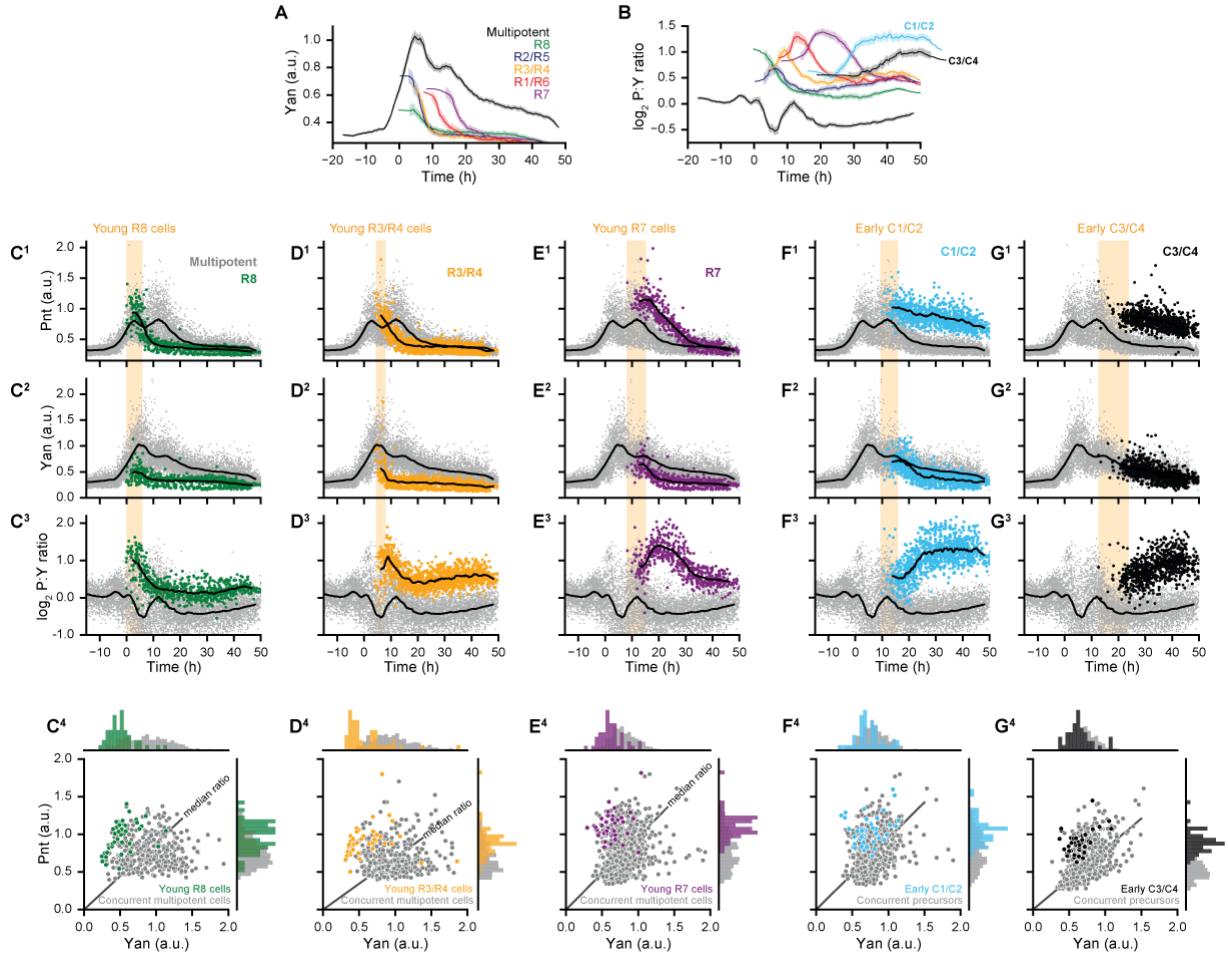

Figure S2:

(A,B) Measured expression dynamics for all annotated cell types. Solid lines are moving averages across 250 and 75 sequential cells for progenitors and differentiating cells, respectively. Shading denotes bootstrapped 95% confidence interval for the moving average. Colors denote cell type.

(C-E) Expression dynamics and joint Pnt-Yan distributions for differentiating R8, R3/R4, and R7 cells. Joint distributions are limited to multipotent and R cells drawn from the shaded yellow region spanning the first ten R cells of the specified type in each disc. Solid lines are smoothed moving averages across 250 and 50 samples for multipotent and R cells, respectively.

(F-G) Expression dynamics and joint Pnt-Yan distributions for differentiating C1/C2 and C3/C4 cone cells.

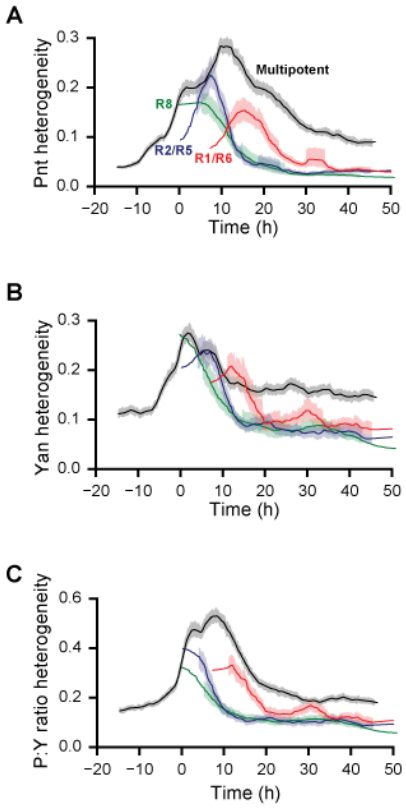

Figure S3:

(A-C) Dynamics of expression variability in multipotent and R8, R2/R5 and R1/R6 cells. Heterogeneities of (A) Pnt expression, (B) Yan expression, and (C) the $\log_2$-transformed ratio are estimated by de-trending fluctuations about a moving average of 250 sequential cells. Lines are moving averages of 250 sequential fluctuations, shaded regions are bootstrapped 95% confidence intervals for the moving average. Colors denote cell type.

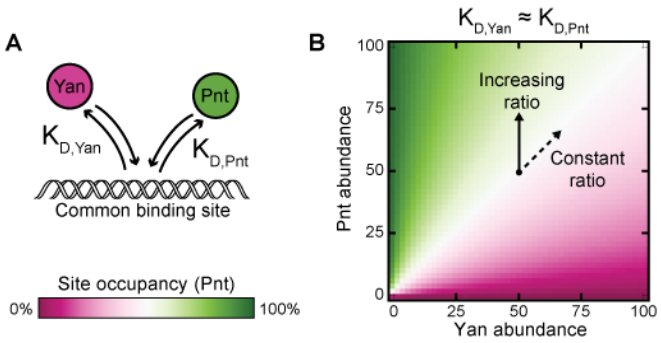

Figure S4:

(A) Schematic of a simple two-species competitive binding model.

(B) Theoretical Pnt site occupancy as a function of transcription factor abundance. Equivalent binding affinities are used for illustrative purposes. Simultaneous proportional increases in absolute abundance of both species have minimal impact on Pnt occupancy, while varying ratio confers maximal change.

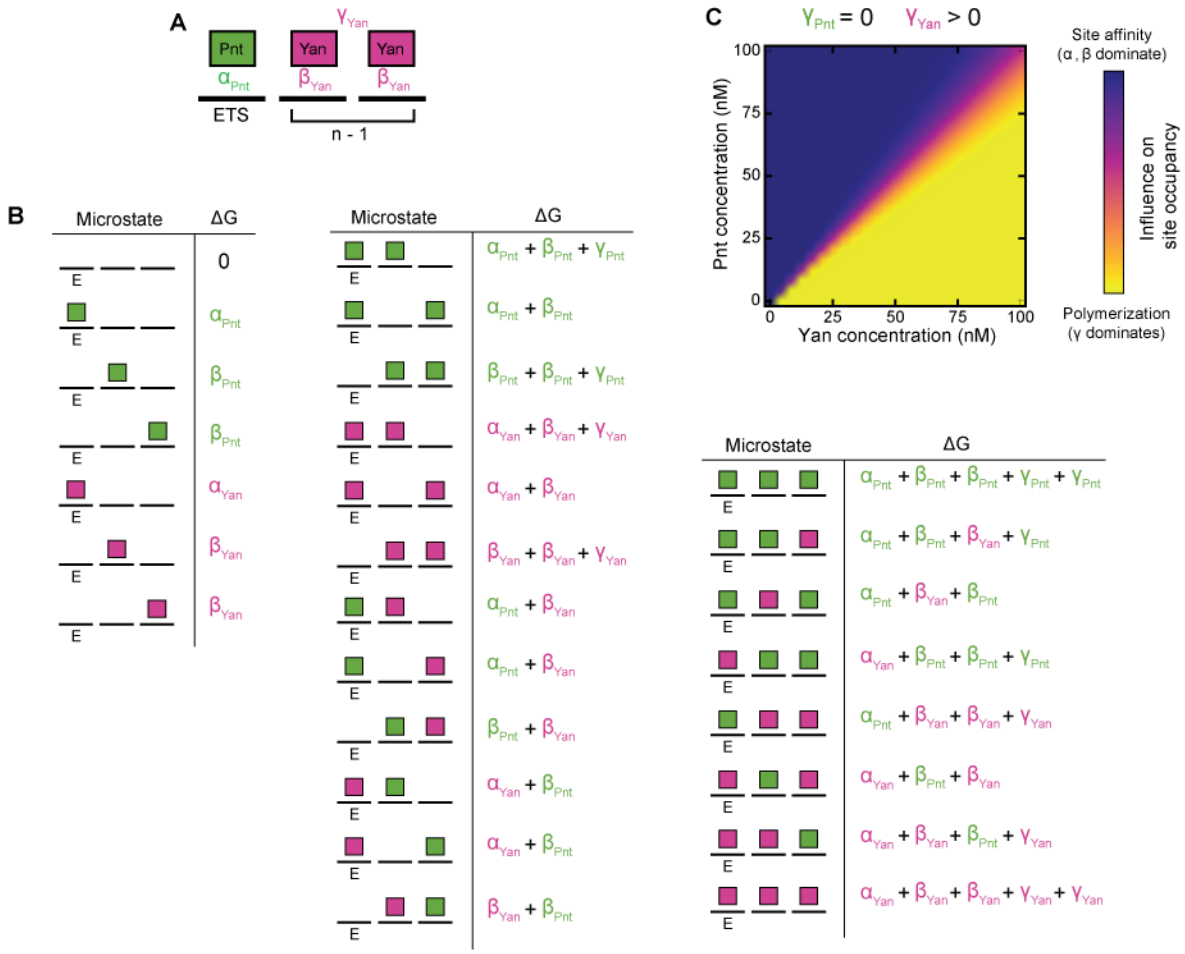

Figure S5:

(A) Summary of thermodynamic interactions within one microstate of a cis-regulatory element containing one ETS site and two non-ETS sites. Solid black lines represent individual binding sites. Green and magenta rectangles denote Pnt and Yan molecules. Example thermodynamic potentials of strong ETS-binding, weak non-ETS binding, and polymerization interactions are denoted by α_{Pnt}, β_{Yan}, and γ_{Yan}, respectively. For this microstate, $a_P(k)$=1 and $a_Y(k)$=2.

(B) Enumeration of all possible microstates for a cis-regulatory element of length 3 in which only the first site carries the ETS designation. Solid black lines denote binding sites, green and magenta rectangles denote bound Pnt and Yan molecules. The cumulative thermodynamic potentials of each microstate, ΔG_k, are listed beside each graphical depiction.

(C) Relative thermodynamic contributions of binding site affinity versus polymerization to microstate statistical frequencies as a function of Pnt and Yan concentration. For each point in the plane, influence of site affinity was calculated by weighting the sum of all ETS and non-ETS thermodynamic potentials for each microstate by the statistical frequency of the corresponding microstate. The influence of polymerization was analogously determined. The shown color scale reflects the relative magnitude of these two summations, normalized by limits of zero and complete polymerization.

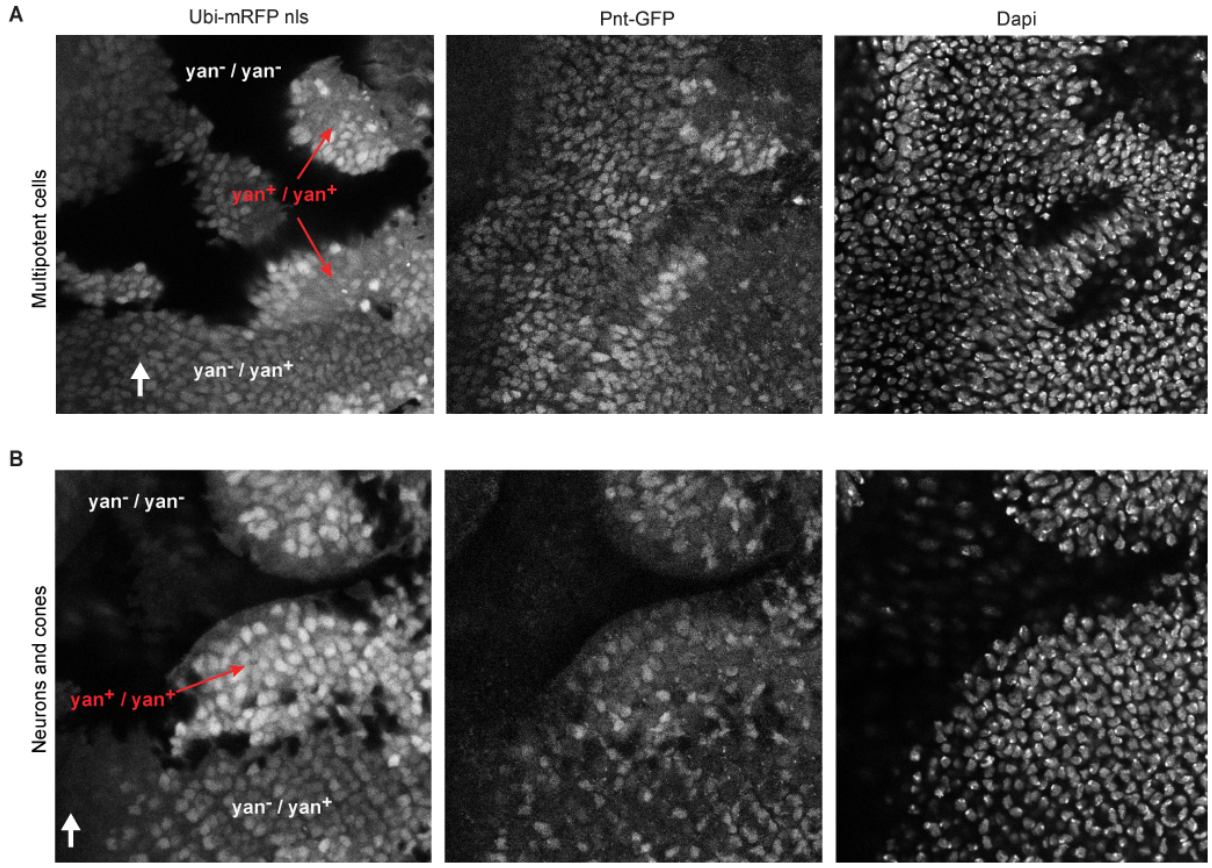

Figure S6:

(A, B) Confocal images of (A) multipotent cells and (B) neurons and cone cells in *yan* null and heterozygote clones. Regions of Ubi-mRFPnls expression are manually labeled by *yan* genotype. White text indicates regions of reduced *Yan* abundance, red denotes wildtype. DAPI is expressed in all nuclei.

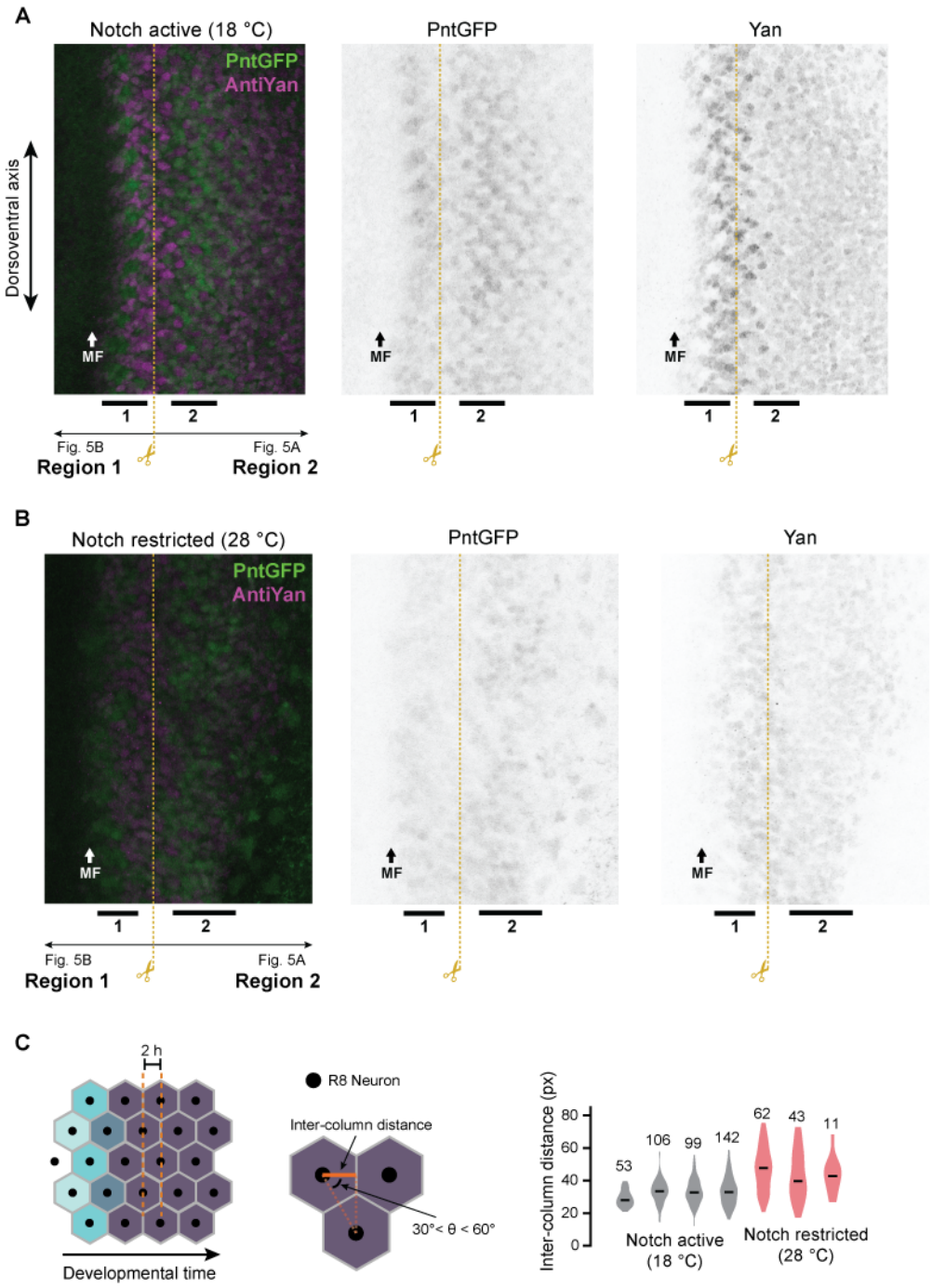

Figure S7:

(A, B) Maximum intensity projections across confocal layers spanning multipotent cells when Notch signaling is (A) active and (B) restricted. Middle and right panels show Pnt-GFP and Yan expression, left panel shows merge in which Pnt-GFP is green and Yan is magenta. Black bars denote first and second periods of elevated Pnt-GFP expression. Dashed yellow line indicates crop boundary used to construct Figures 5A and 5B.

(C) Distances between adjacent ommatidial columns in Notch mutant discs. Left panel: Procedure used to estimate inter-column distance. Neighboring R8 cells are identified by Delaunay triangulation, with an added constraint that edges must fall within 30 to 60 degrees of the

anterior-posterior axis. The inter-column distance is estimated by averaging the anterior-posterior distance between neighbors (solid orange line). Right panel: Inter-column distances are more variable when Notch signaling is restricted (red) than under wildtype (grey) conditions. Black bars denote median, numbers above violins indicate the number of neighboring R8 cells. High variability prevents accurate estimation of MF velocity and precludes conversion of spatial positions to developmental times.

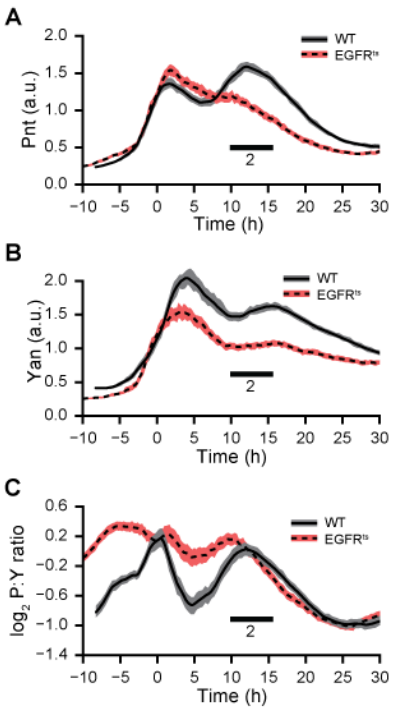

Figure S8:

(A-C) Effects of restricted RTK signaling on (A) Pnt-GFP, (B) Yan, and (C) Pnt-to-Yan ratio dynamics in multipotent cells. Lines are moving averages across 250 sequential cells. Shaded regions are bootstrapped 95% confidence intervals for the mean. Solid lines and grey shading denote wildtype controls. Dashed lines and red shading denote restricted RTK signaling. Black bars denote second period of elevated Pnt-GFP expression.

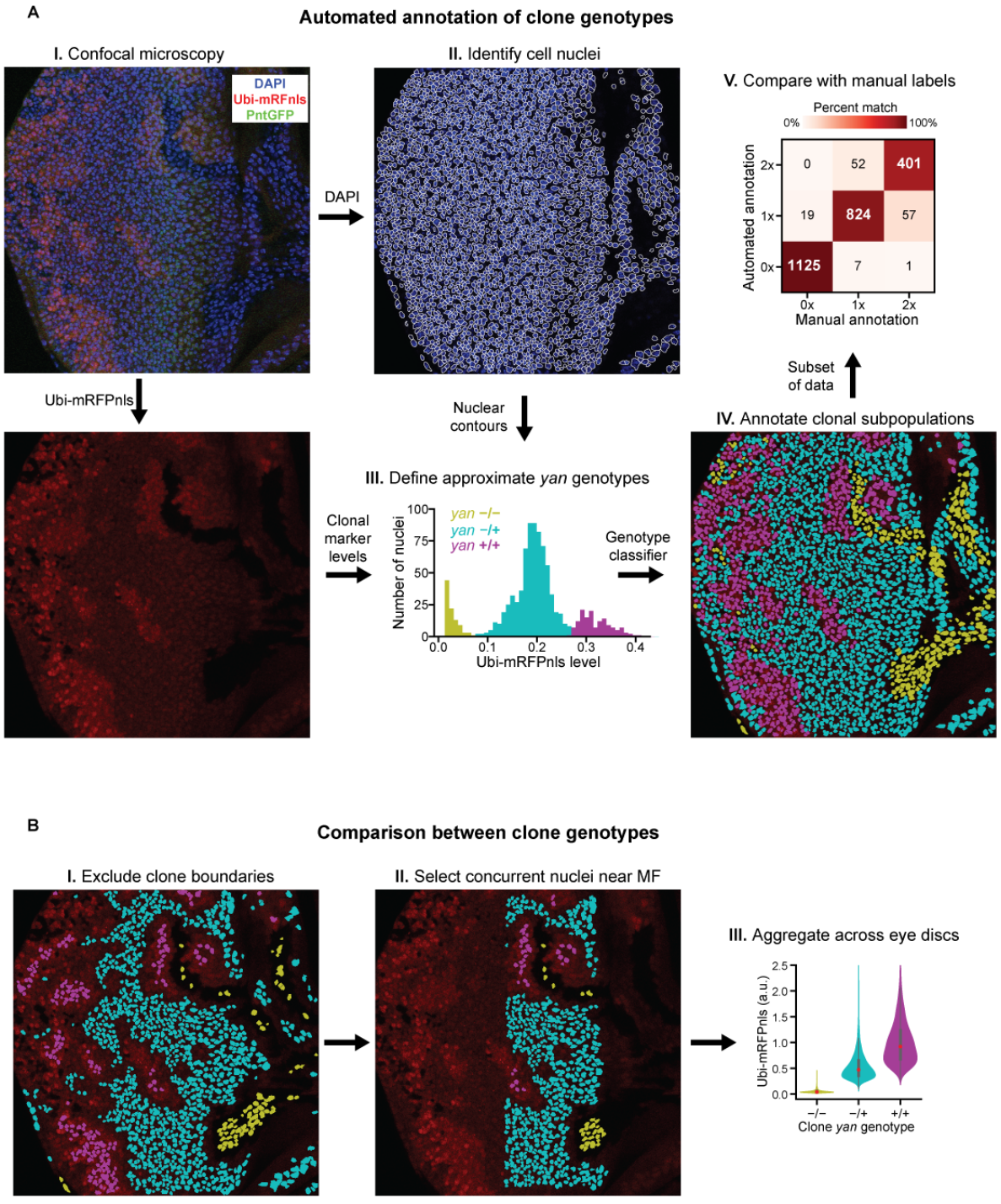

Figure SI-1:

(A) Computational pipeline for automated annotation of clonal subpopulations. (I) Example image of multipotent cells in an eye disc containing *yan* null clones. (II) Watershed segmentation of a distance-transformed foreground mask of the DAPI fluorescence channel yields contours surrounding each cell nucleus. (III) Histogram of measured Ubi-mRFPnls levels within the image. Colors denote genotypes assigned by a k-means classifier. Additional clusters were manually added and merged where necessary in order to obtain reasonable thresholds

between genotypes. (IV) Completed annotation of the example image. Segment colors reflect the final genotype assigned to each cell segment. Yellow, cyan, and magenta correspond to 0x, 1x, and 2x *yan* genotypes, respectively. (V) Comparison with *yan* genotype labels manually assigned to ~2500 cells in four eye discs. Numbers denote the number of cells within each bin and the color scale denotes the overlap between bins. Overall misclassification rate is ~5%, with most errors occurring between cells with one or two copies of *yan*.

(B) Procedure for selection, aggregation, and comparison of clonal subpopulations. Colors retain their meaning from panel A. (I) Cell segments bordering each clone are excluded from the analysis. (II) Analysis is limited to cells coinciding with the two peaks of PntGFP immediately posterior to the morphogenetic furrow. (III) Cell measurements are aggregated across multiple layers of multiple eye discs yielding statistical comparisons between clonal genotypes.

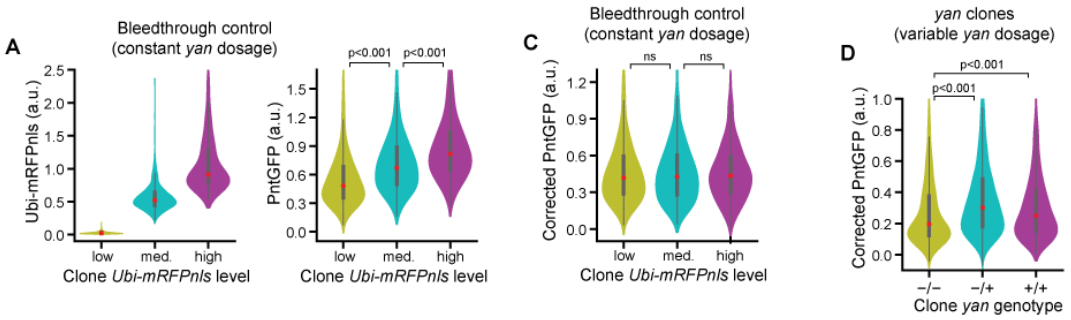
A
Bleedthrough control
(constant yan dosage)
Ubi-mRFPnls (a.u.)
PntGFP (a.u.)
p<0.001
p<0.001
low
med.
high
Clone Ubi-mRFPnls level
C
Bleedthrough control
(constant yan dosage)
Corrected PntGFP (a.u.)
ns
ns
Clone Ubi-mRFPnls level
D
yan clones
(variable yan dosage)
p<0.001
p<0.001
−/−
−/+
+/+
Clone yan genotype

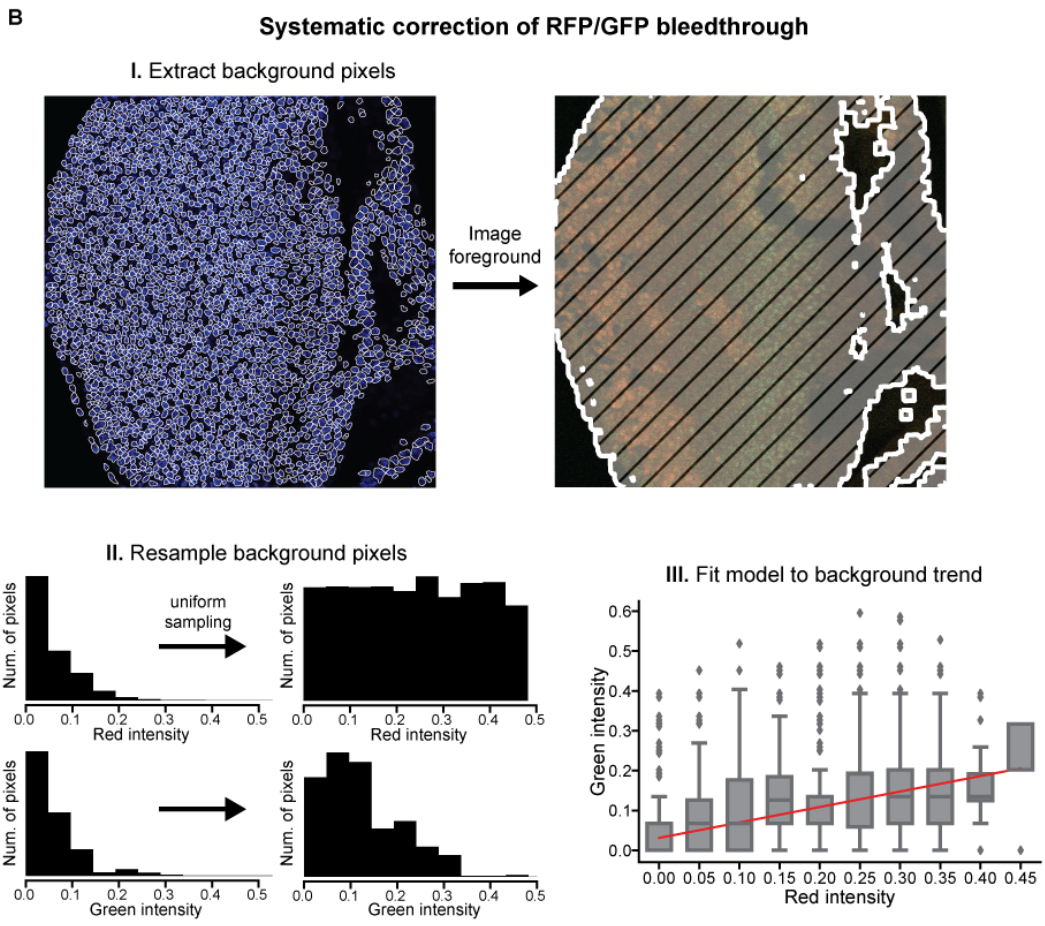
B
Systematic correction of RFP/GFP bleedthrough
I. Extract background pixels
Image foreground
II. Resample background pixels
uniform sampling
Num. of pixels
Red intensity
Green intensity
III. Fit model to background trend
Green intensity
Red intensity
IV. Subtract background trend from GFP measurements
Measured GFP level
Measured RFP level
Corrected GFP level

Figure SI-2:

(A) Comparison of measured Ubi-mRFPnls and PntGFP levels between annotated clone genotypes in bleed-through control clones. Measured PntGFP levels are correlated with measured Ubi-mRFPnls levels despite all cells containing the same number of copies of the *yan* gene. p-values are derived from Mann-Whitney *U* tests.

(B) Procedure for systematic correction of RFP/GFP bleed-through applied to an example image of an eye disc containing *yan* clones. (I) Background pixels are obtained by dilating a binary foreground mask until no image features remain visible. Left panel shows cell contours (foreground) superimposed on the DAPI channel of an example disc. Right panel shows dilated foreground (hashed area) superimposed on the RFP and GFP channels. (II) Background pixels are resampled such that the resultant distribution of measured RFP levels is approximately uniform. (III) A generalized linear model with gamma-distributed residuals and an identity link function is fit to the intensities of the resampled pixels' RFP and GFP channels. Data are binned for ease of visualization, red line reflects model fit. (IV) Correction of measured GFP levels (black markers) for all cells in the example image. Left and right panels show original and corrected measurements of PntGFP level. The model (red line) clearly tracks the baseline trend in the original measurements, despite only being fit to the image background.

(C) Comparison of corrected PntGFP levels between annotated clone genotypes in bleed-through control clones. Corrected PntGFP levels are statistically indistinguishable between annotated genotypes ($p>0.5$, Mann-Whitney *U* tests).

(D) Comparison of corrected PntGFP levels between annotated clone genotypes in *yan* null clones. PntGFP levels are higher in multipotent cells with one or two copies of *yan* than in cells with no copies ($p<0.001$, Mann-Whitney *U* tests).